IEEE Open Journal of the
Industrial Electronics Society

Received 19 June 2020; revised 7 August 2020; accepted 9 August 2020. Date of publication 12 August 2020;
date of current version 4 September 2020. The review of this article was arranged by Associate Editor Dr. Yushan Liu.

Digital Object Identifier 10.1109/OJIES.2020.3016242

Electromagnetic Modeling Techniques for Switched Reluctance Machines: State-of-the-Art Review

GAYAN WATTHEWADUGE (Member, IEEE), EHAB SAYED (Member, IEEE), ALI EMADI (Fellow, IEEE), AND BERKER BILGIN (Senior Member, IEEE)

Department of Electrical and Computer Engineering, McMaster University, Hamilton, ON L8S 4K1, Canada

CORRESPONDING AUTHOR: BERKER BILGIN (e-mail: bilginb@mcmaster.ca)

This work was supported by the Natural Sciences and Engineering Research Council of Canada (NSERC).

ABSTRACT Switched Reluctance Machines (SRMs) are gaining more attention due to their simple, and rugged construction, low manufacturing cost, and high-speed operation capability. An electromagnetic model of the machine is needed in the design, and analysis processes. The required accuracy level of the model depends mainly on the application. A high-fidelity model is required to achieve a good design, and predict the performance accurately. However, it requires high computational cost, and longer simulation time. Other fast, and less-comprehensive models with less computational burden could be utilized in the design, and analysis of the motor drives. This paper extensively analyzes various electromagnetic modeling techniques of SRMs. Analytical, numerical, and hybrid models are considered. The paper investigates analytical models that are based on Maxwell's equations in addition to interpolation, and curve fitting techniques. Numerical techniques such as Finite Element Method (FEM), and Boundary Element Method (BEM) are presented. Moreover, Magnetic Equivalent Circuit (MEC) method is discussed. Finally, potential research areas are proposed for the electromagnetic modeling of SRMs.

INDEX TERMS Analytical model, boundary element method (BEM), electromagnetic modeling, finite element method (FEM), magnetic equivalent circuit (MEC) model, numerical model, switched reluctance machine (SRM).

I. INTRODUCTION

SRM is an emerging and competitive alternative to permanent magnet (PM) machines. This is due to their simple and rugged construction, lower cost, high-speed operation capability, and lack of PMs [1]–[3]. SRMs are commonly utilized in various industrial applications such as pumps and fans and, have a high potential to be used in future electric traction systems [1]–[3]. Although PM machines play a vital role in electrified transportation systems, the magnet-free SRMs are becoming more attractive. Extensive research is conducted to solve the high torque ripple, high acoustic noise, and low torque density issues in SRMs [1], [3]. The Axial flux SRM is suitable for in-wheel traction drives, as it can provide higher torque density as compared to its radial flux counterpart [4]–[7].

Design and analysis of electric machines require an electromagnetic model [8]. The model provides various key electromagnetic performance characteristics such as magnetic flux density, magnetic field intensity, induced electromotive force, and electromagnetic torque. The model could also estimate the machine losses such as AC copper loss, hysteresis loss, and eddy-current loss. In addition, it could be utilized within an optimization process to achieve different objectives such as to minimize the torque ripple [9], maximize the efficiency, and minimize the motor weight [10]. Moreover, it helps in the design of the motor drive system [11], [12].

This paper investigates various electromagnetic modeling techniques for SRMs. Analytical, numerical, and hybrid models are considered. The work investigates analytical models that are based on Maxwell's equations in addition to

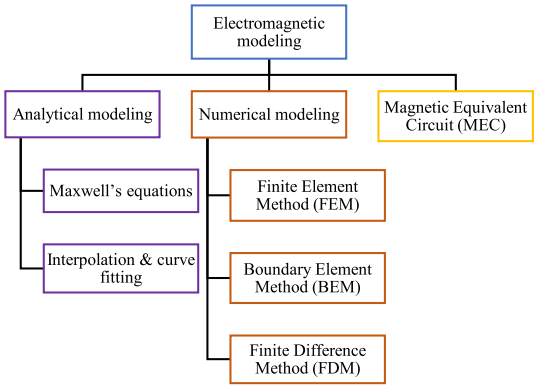

FIGURE 1. **Electromagnetic modeling techniques of electric machines.**

interpolation and curve fitting techniques. Numerical techniques such as Finite Element Method (FEM) and Boundary Element Method (BEM) are studied. Moreover, Magnetic Equivalent Circuit (MEC) method is discussed [13], [14].

The rest of the paper is organized as follows. A general discussion of the electromagnetic modeling techniques of electric machines is presented in Section II. In Section III, the discussion is narrowed down to review the analytical modeling techniques for SRMs. Numerical modeling techniques for SRMs are presented in Section IV, and the MEC method is discussed in Section V. A discussion on the potential research areas of SRM modeling is investigated in Section VI. Finally, the conclusions are presented in Section VII.

II. MODELING TECHNIQUES FOR ELECTRIC MACHINES

Electromagnetic modeling of electric machines can be divided into two main categories (i) analytical modeling and (ii) numerical modeling. Each category comprises sub-categories as shown in Fig. 1 [13]. Analytical techniques have major challenges in approximating a complex geometry, considering core saturation, calculating the hysteresis and eddy current losses in the core, modeling the skin and proximity effects in the winding, and modeling the end-winding inductance [13], [15]. However, analytical models are computationally cheap compared to numerical models [13]. The most common analytical models are based on Maxwell's equations or interpolation and curve fitting techniques. In Maxwell's-equations-based models, the differential equations are analytically solved by neglecting the local saturation, the effect of mutual coupling, and leakage flux. This reduces the model accuracy [16], [17]. The Maxwell's equations based analytical models are preferred in initial design stages to estimate the main design parameters [18], [19]. The interpolation- and curve-fitting-based techniques are another approach to model SRMs. They include experimental or Finite Element (FE) model data to develop the model. However, new data is required if the machine geometry changes. Thus, these models are more suitable for designing the controllers of motor drive systems.

Various numerical techniques are utilized in modeling electric machines such as FEM, BEM, and Finite Difference Method (FDM). FEM is the most common numerical technique due to its high accuracy [20], [21]. It can accurately estimate various electromagnetic characteristics considering complex geometries and nonlinearity of the core materials, where the material relative permeability depends on the magnetic flux density [20]. In [20], the FEM was utilized to solve low frequency saturable electromagnetic field problems. Two-dimensional (2D) FE model was introduced in [20] and [21] to calculate the electromagnetic fields in electric machines. FEM is currently utilized to model complex geometries of electric machines considering skin, and proximity effects, and 3-dimensional (3D) effects. It also helps estimating the machine losses. However, the FE models have high computational cost and, depending on the complexity of the problem, the simulation time might takes hours to finish. BEM can be utilized as an alternative to FEM, since it introduces less computational burden. The problem domain is reduced from 3D to 2D in BEM [14]. However, BEM is difficult to apply to solve saturable electromagnetic fields since the coefficient matrices are not symmetric, not positive definite and completely populated [21], [22]. FDM is another option to model electric machines. However, it has difficulties in modeling complex geometries; therefore, it is not directly applied to model electric machines [21]. FDM is extended to define another technique called reluctance mesh approach that can also be categorized under the MEC method [22], [23].

The MEC modeling is a popular method in modeling electric machines [13]. It is a special case since it can be considered as an analytical or a numerical technique according to how it is applied. It is considered as an analytical technique if it is combined with other analytical modeling techniques such as Maxwell's equations [24], [25]. When the nonlinearity of the magnetic materials is considered, the MEC modeling has to be combined with numerical techniques [26]. In [26], the MEC method was applied to calculate the magnetic flux in toroidal-core and C-core magnetic devices. The method has been applied in [26] to model magnetic devices with moving parts.

In the MEC method, an electric circuit model is developed to analyze the magnetic characteristics of a system by utilizing the analogy between magnetic and electric circuits presented in Table 1. A simple magnetic device that comprises a toroid with two air gaps is illustrated in Fig. 2(a). The corresponding MEC is shown in Fig. 2(b). The MEC in Fig. 2(b) has four reluctances: two reluctances for the core parts (R_{c1}, R_{c2}) and two reluctances for the airgaps (R_{g1}, R_{g2}). The flux flow in the toroid and airgaps can be considered similar neglecting the leakage flux. The MMF source is calculated by multiplying the winding turns N and the excitation current I. The MEC technique can be improved to model the saturation, leakage flux, and various electromagnetic losses with fair accuracy compared to FEM [13]. The model accuracy increases by adding more reluctance elements. However, this increases the model complexity [26].

TABLE 1. Analogy Between Magnetic and Electric Circuits

Type of the circuit		
Quantity	Magnetic circuit	Electric circuit
Flux/Current density	$\vec{B}$	$\vec{J}$
Field strength	$\vec{H}$	$\vec{E}$
Permeability/Conductivity	μ	σ
Reluctance/Resistance	R_{mag}	R_{elec}
Flux/Current	Φ	I
Magnetomotive/Electromotive force	MMF	EMF
Magnetic/Electric potential	U	V
Hopkinson's/Ohm's law	$U = \Phi R_{mag}$	$V = IR_{elec}$
Magnetic/Electric energy	$U\Phi$	VI

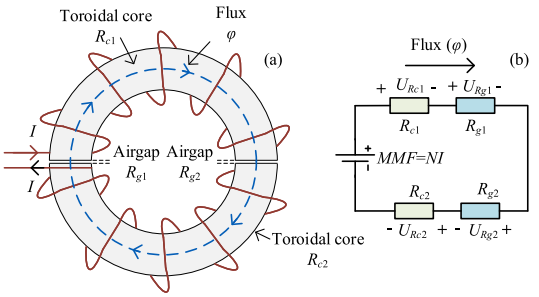

FIGURE 2. (a) A toroidal core and (b) the corresponding MEC.

Narrowing the discussion from electric machines to SRMs, the modeling techniques can still be categorized according to the previous classification [14], [27]. The main objective of electromagnetic modeling of SRMs is to obtain the machine phase flux linkage as a function of the stator current and rotor position [14]. Then, other electromagnetic characteristics can be predicted using (1)-(3). The variables ψ, i, V, R, T_e, W_c, and θ_r are the phase flux linkage, phase current, phase voltage, phase resistance, electromagnetic torque, magnetic co-energy, and rotor position, respectively [14], [28].

$$\frac{d\psi(i,\theta_r)}{dt} = V - Ri \tag{1}$$

$$W_c = \int_0^i \psi(i,\theta_r)di \tag{2}$$

$$T_e = \frac{\partial W_c}{\partial \theta_r} \tag{3}$$

An ideal phase flux linkage characteristic of SRMs is illustrated in Fig. 3. The variables α_1, α_2, and N_r are $(\beta_r - \beta_s)/2$, $(\beta_r + \beta_s)/2$, and the number of rotor poles, respectively. β_s and β_r are the stator and rotor pole arc angles, respectively. As shown in the Fig. 3, three main regions are identified based on the rotor position. These positions are the aligned position, partial-overlap position, and unaligned position as shown in Fig. 4. At the aligned position, the rotor pole fully overlaps the excited stator pole, whereas it partially overlaps the stator pole in the partial-overlap position as shown in Fig. 4(b). There is no overlap between the rotor poles and the excited stator pole

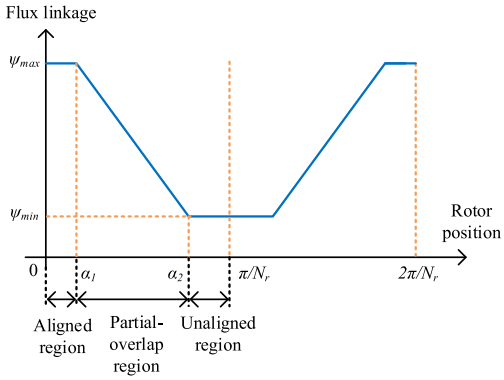

FIGURE 3. An Ideal phase flux linkage characteristic versus rotor position.

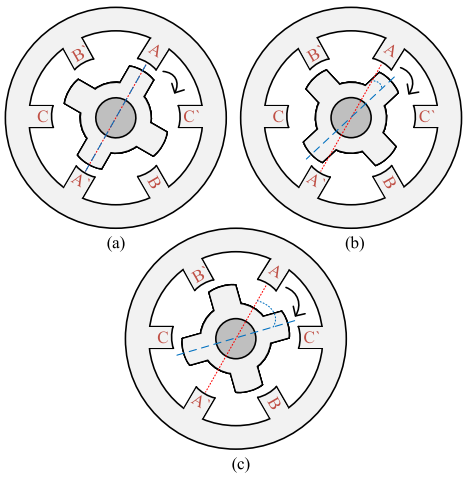

FIGURE 4. Different rotor positions of SRM (a) aligned, (b) partial-overlap, and (c) unaligned.

at the unaligned region as shown in Fig. 4(c). It should be indicated that the phase inductance profile follows a similar pattern to that of the flux linkage. A high phase inductance exists at the aligned position since the flux path reluctance is minimum. The inductance drops as the rotor moves from the aligned position to the unaligned position since the reluctance increases. Modeling of SRMs is challenging due to many reasons. The phase flux linkage is a nonlinear function of the rotor position and the stator excitation current [14], [28], and the machine commonly works in a saturated condition. Moreover, the airgap periphery is irregular due to the doubly-salient structure of the machine. Hence, various modeling techniques can be applied to SRMs.

III. ANALYTICAL MODELING TECHNIQUES FOR SRMS

Analytical modeling techniques, shown in Fig. 1, can be extended further as shown in Fig. 5. The interpolation-and-curve-fitting-based techniques are divided into four subcategories, where they rely on lookup tables, linear/nonlinear curve fitting, Fourier series, or artificial intelligence.

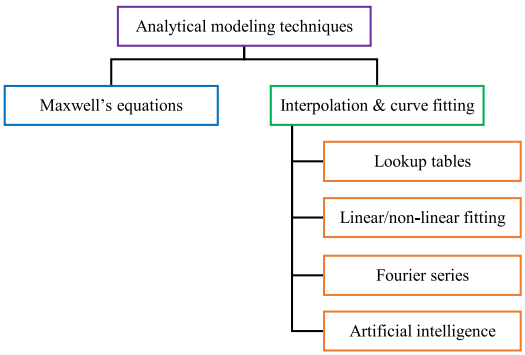

FIGURE 5. Various types of analytical methods for SRM modeling.

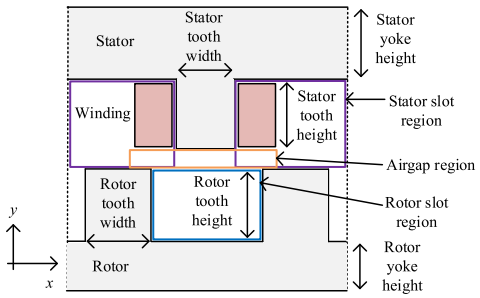

FIGURE 6. Formulation of a rectangular-shaped Boundary Value Problem (BVP) by unwrapping the circular SRM shape [30].

A. MAXWELL'S-EQUATIONS-BASED METHODS

The partial differential equations, formulated using Maxwell's equations, are solved using analytical methods. The magnetic vector potential or magnetic scalar potential inside the SRM boundary is determined by solving these differential equations [20]. Poisson's equation of magnetic vector potential $\vec{A}$ is

$$\nabla^2 \vec{A} = -\mu \vec{J} \tag{4}$$

where $\vec{J}$ and μ are current density vector and permeability of the material, respectively. Equation (4) is derived assuming the material is isotropic and linear. Therefore, the permeability of the material does not depend on the flux density, and has no spatial variation. Alternatively, the magnetic field can be solved by using magnetic scalar potential U under the same assumptions [21], [29]. Poisson's equation of U can be obtained as

$$\nabla^2 U = \nabla \cdot \vec{T} \tag{5}$$

where $\vec{T}$ is the electric vector potential. The equations (4) [30] or (5) [21], [31] can be solved analytically as a Boundary Value Problem (BVP) to calculate the magnetic vector potential or magnetic scalar potential. There are several ways to solve this BVP. The most common approaches are variable separable method [30], [32] and conformal mapping [31], [33]–[35].

As shown in Fig. 6, the circular geometry of the SRM can be approximated as 2D unwrapped rectangular shape in the x-y plane. However, this approximation can introduce errors due to inconsistency in the geometry. These modeling errors in the calculation of the magnetic field of an SRM can be reduced by solving the Poison or Laplace equation in the cylindrical domain as shown in Fig. 7. A major assumption in the field calculation is that an infinite permeability is considered for the iron core. Thus, $\vec{H}$ field inside the stator and rotor core becomes zero. The geometry inside the air region can be divided into three parts as in Fig. 6 and Fig. 7: Airgap region, stator slot region, and rotor slot region [36]. The vector $\vec{T}$ in the rotor slots and airgap regions is zero due to zero current density in these regions. Hence, (5) transforms to a Laplace equation and the variable separable method can be applied within the boundaries as shown in Fig. 6 and Fig. 7 to calculate U. The magnetic field inside the stator slot region can be calculated by solving (4) using the variable separable method inside the defined boundaries in Fig. 6 and Fig. 7.

In conformal mapping technique, the Schwartz-Christoffel (SC) transformation is applied to transform a complicated geometry into a simple one, which makes the magnetic field calculation easier [31], [33], [34], [37]. This technique was applied to calculate the airgap magnetic field [33] of SRMs. The transformation process is illustrated in Fig. 8 [33], [37].

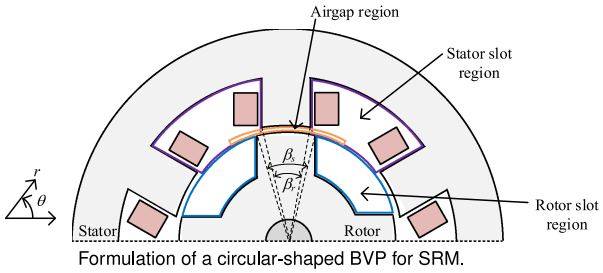

FIGURE 7. Formulation of a circular-shaped BVP for SRM.

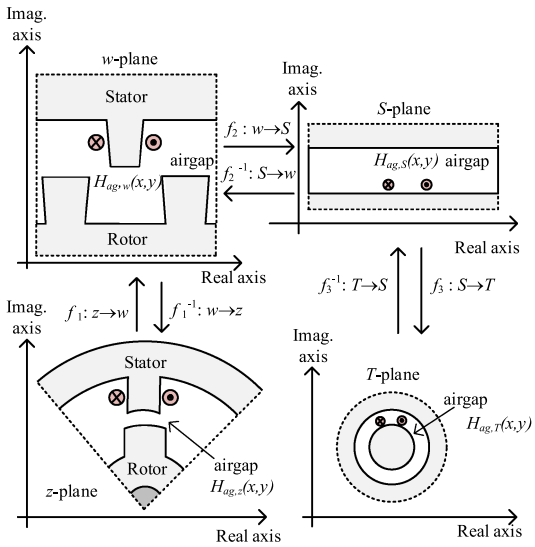

FIGURE 8. Schwarz-Christoffel transformation of SRM domain [33], [37].

The circular geometry of the SRM is represented in the complex z-plane. Then, a logarithmic Conformal Mapping (CM) is applied to transform the geometry from the z-plane to the w-plane. This results in a rectangular shape SRM geometry with trapezoidal shape stator and rotor poles. The SC transformation is applied again to transform the geometry from the w-plane to the S-plane, which results in a canonical rectangular shape. Finally, an exponential CM is applied again to transform the geometry from the S-plane to the T-plane, which results in an annular shape. The solution of the magnetic field $\vec{H}_{ag,T}(x, y)$ in the airgap in the T-plane is obtained by Hague's equation [33]. Once $\vec{H}_{ag,T}(x, y)$ is calculated, the inverse transformations are applied to obtain the electromagnetic field in the airgap in the z-plane. The SC techniques is highly accurate in the linear regions of the magnetic materials and useful for analyzing the 2D electromagnetic characteristics of SRMs. However, this technique cannot be applied for 3D modeling and, with this method, it is more challenging to take the local saturation into account.

B. INTERPOLATION- AND CURVE-FITTING-BASED METHODS

These methods are popular in the design and development of SRM drives [38]. Phase flux linkage/inductance and torque characteristics as functions of the rotor position and the stator current are necessary to develop the models. Numerical simulation data, mostly based on Finite Element Analysis (FEA) or experimental results are utilized [14]. The phase flux linkage of SRMs can be estimated experimentally at different rotor positions and different excitation currents [39]–[43]. The flux linkage is the integral of the machine EMF which is estimated based on the measured winding resistance, current, and voltage. The torque can be measured using a torque sensor or estimated by applying (1) to (3) to the mentioned measurements. FE simulations can also be used to obtain the flux linkage and torque characteristics. Preparing the experimental or the FE data takes significant time, and the developed model will be valid only for the given geometry and the configuration.

The flux linkage and torque data can be used in the form of look-up tables, linear/nonlinear curve-fitting formulas, Fourier series, and artificial intelligence [38], [44].

1) LOOK-UP TABLES

This technique is simple to implement with good accuracy using tools such as MATLAB, OCTAVE, and Compose and Activate by Altair [41], [42], [45], [46]. The machine phase flux linkage/inductance and torque characteristics at different stator currents and different rotor positions are saved in 2D lookup tables. The torque and flux linkage/inductance values in the model are then obtained based on the input rotor position and excitation. Interpolation is applied between the existing data. Lookup tables developed by running FEM simulations of an 8/6 SRM model are illustrated in Fig. 9.

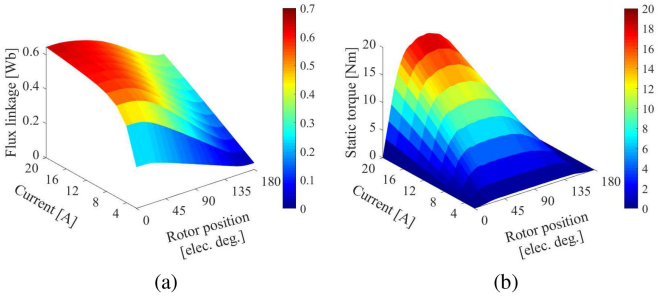

FIGURE 9. **SRM lookup tables obtained form FE simulations (a) flux linkage versus rotor position and current and (b) torque versus rotor position and current.**

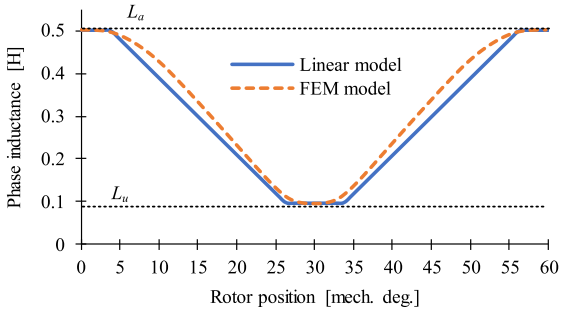

FIGURE 10. **Inductance profile of an 8/6 SRM developed using piecewise linear function and FEM.**

2) LINEAR/NONLINEAR CURVE-FITTING FORMULAS

In this technique, the formulas of the machine phase inductance/flux linkage and torque are utilized as functions of the rotor position and stator current [47]. The least square technique is applied to fit the simulation or experimental data to these formulas. The phase inductance profile, as an example, can be simply approximated as a piecewise linear function [48]

$$L(\theta_r) = \begin{cases} L_a; & 0 \le \theta_r \le \alpha_1 \\ L_a - K(\theta_r - \alpha_1); & \alpha_1 \le \theta_r \le \alpha_2 \\ L_u; & \alpha_2 \le \theta_r \le \frac{2\pi}{N_r} - \alpha_2 \\ L_a + K(\theta_r - \frac{2\pi}{N_r} + \alpha_1); & \frac{2\pi}{N_r} - \alpha_2 \le \theta_r \le \frac{2\pi}{N_r} \end{cases} \tag{6}$$

where the constant K is given by $(L_a - L_u)/\beta_s$. The L_a is the inductance at the aligned position and L_u is the minimum inductance at unaligned position. The angles α_1 and α_2 were shown in Fig. 3. N_r is the number of rotor poles. Fig. 10 shows an SRM inductance profile developed using (6) and using FEM. Although the approximation is reasonable, there is some difference between the two profiles. The linear inductance profile in Fig. 10 is developed for a 8/6 SRM. The FE model of the 8/6 SRM is developed using ANSYS Maxwell software. Similarly, the flux linkage versus current profile can be approximated as linear piecewise functions [48], [49]. Different piecewise functions can be developed at different rotor

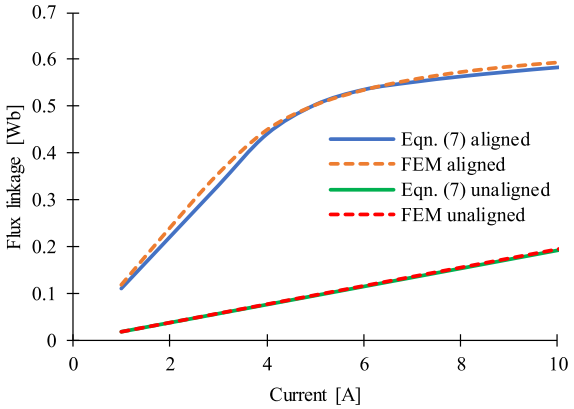

FIGURE 11. Comparison of the flux linkage profile of an 8/6 SRM developed using the nonlinear function in (7) against FEM.

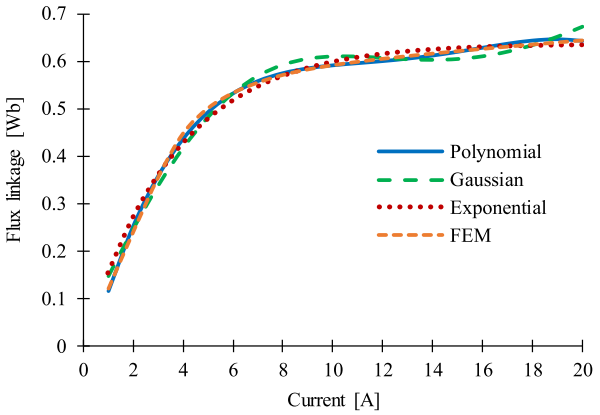

FIGURE 12. Comparison of different curve fitting techniques for modeling flux linkage characteristics of an 8/6 SRM.

position ranges. Piecewise nonlinear functions [50]–[52] such as parabolic function [52] can also be applied. The flux linkage versus current characteristic at the aligned and unaligned rotor positions can be approximated as [52]

$$\psi(i) = \begin{cases} L_u i; & \text{unaligned} \\ L_{a,0} i; & \text{aligned } (i \le i_s) \\ \psi_0 + \sqrt{4a(i - i_0)}; & \text{aligned } (i > i_s) \end{cases} \quad (7)$$

where a, ψ_0, and i_0 are constants that are determined using simulation or experimental data. The flux linkage profile is linear at the unaligned position. However, for the aligned position, a linear flux linkage can be considered only up to a certain excitation current i_s [52]. Therefore, $L_{a,0}$ is the inductance at the aligned position when $(i \le i_s)$. The flux linkage is nonlinear when $(i \ge i_s)$, as shown in Fig. 11. The representation matched the FEM profile well at the unaligned position, whereas there are some discrepancies at the aligned position. The same 8/6 SRM is utilized in here to obtain the flux linkage profiles in Fig. 11. Alternatively, various 2D polynomials such as bivariate polynomials and bi-cubic spline polynomials can be utilized to model the flux linkage and torque characteristics of an SRM [53], [54]. Curve fitting techniques based on off-line and online least square method can be used to determine the coefficients of the polynomials [53]. A 2D orthogonal polynomial of the flux linkage as a function of the rotor position and the stator current is expressed as [53]

$$\psi(i, \theta_r) = \sum_{m=0}^{k-1} \sum_{n=0}^{r-1} a_{mn} (\theta_r - \bar{\theta})^m (i - \bar{i})^n \quad (8)$$

where a_{mn} is a constant. k and r are positive integers such that $k \times r$ equals the number of available data points. The parameters $\bar{\theta}$ and $\bar{i}$ are the mean values of the rotor position data and current data, respectively [55]. Additionally, other nonlinear functions such as Gaussian functions [56], piecewise Frohlich functions [57], and exponential functions [55], [58], [59] could be utilized to approximate the flux linkage

TABLE 2. RMSE Comparison Between Interpolation- and Curve-Fitting Techniques With Respect to FEM Results

Modeling technique	RMSE
Eqn. (7)	3.34%
Polynomial	1.67%
Gaussian	5.84%
Exponential	7.33%

profiles. Fig. 12 shows the developed flux linkage profiles using 2D orthonormal polynomial [53], Gaussian function [56], and exponential function [55]. The profiles are compared with that obtained using the FEM model of the same 8/6 SRM. Table 2 shows the root-mean-squared-error (RMSE) of the flux linkage profiles obtained from nonlinear curve-fitting formulas with respect to FEM results at the aligned position. The orthonormal-polynomial representation has the lowest RMSE.

3) FOURIER SERIES

Fourier decomposition method can be utilized to represent the machine phase flux linkage/inductance and torque profiles as functions of the stator current and rotor position. It has been extensively applied to SRM modeling [60]–[68]. Considering that an infinite series is not practical, the number of terms is mostly limited between two and four. The accuracy increases as the number of terms increases. The models developed based on Fourier series method can be adaptable to parameter variations due to various losses in SRM, aging, and manufacturing defects [60]. Therefore, these models can be more suitable for controller design in SRM. The inductance profile $L_{ph}(i, \theta_r)$ as a function of the rotor position and stator current can be expanded using Fourier series as follows [63]

$$L_{ph}(i, \theta_r) = \sum_{n=0}^{k_t} L_{ph,n}(i) cos(n(N_r \theta_r + \delta_n)) \quad (9)$$

where $L_{ph,n}(i)$, δ_n, and k_t are the n^{th} Fourier coefficient, phase angle of each Fourier component, and the series truncation

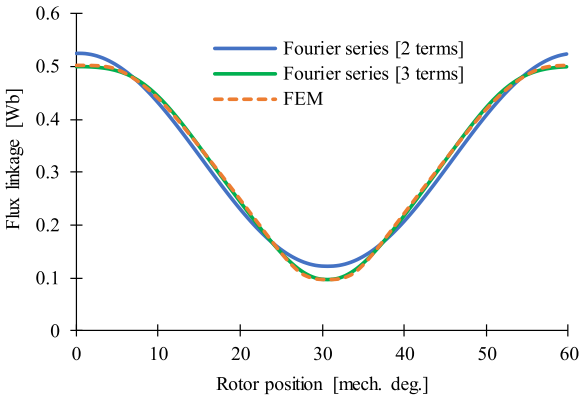

FIGURE 13. **Flux linkage profile versus rotor position developed using Fourier series, eqn. (9), and FEM for the 8/6 SRM.**

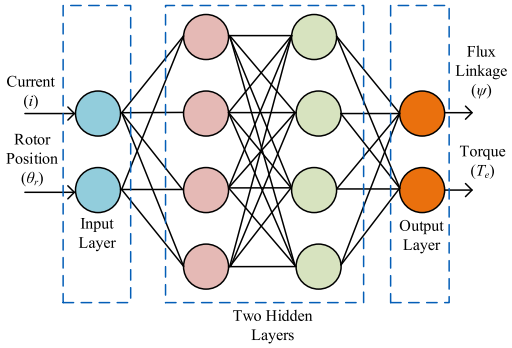

FIGURE 14. **Four-layer Artificial Neural Network for modeling SRMs.**

level, respectively. The flux linkage profile versus rotor position developed using (9) is compared with the FE model of the 8/6 SRM in Fig. 13. There is significant difference between the profiles if only two terms are considered in the Fourier series. The representation is significantly improved when a third term is added. 2D Fourier series can also be utilized to represent the flux linkage characteristics. The phase flux linkage can be expanded as a 2D Fourier series in exponential form [62].

The Fourier coefficients in (9) can be determined using FEA [62], [68], experimental [61] or analytical [60], [63]–[65], [67] techniques. As an example, various analytical techniques such as assuming ideal inductance profile with weighting functions [60], [66], on-line parameter identification techniques [63], [65], polynomial approximations [63], [64] and field reconstruction technique [67] can be applied to determine the Fourier coefficients.

4) ARTIFICIAL INTELLIGENCE

A learning algorithm can be developed to obtain the flux linkage and torque characteristics of an SRM as functions of rotor position and stator current. The Artificial Neural Network (ANN) [69]–[75] and Machine Learning (ML) [76], [77] techniques can be applied to develop this learning algorithm. The key advantage of these techniques is the capability of adapting to parameter variations of the machine due to losses, aging and manufacturing tolerances [69].

ANN has basically three types of layers: input layers, output layers, and hidden layers. Each layer comprises different tiers, which can be considered as a piece of intelligence. The learning rules and algorithms are defined in these tiers. They need to be trained properly to process the given raw data. In case of SRM modeling, there are two main inputs which are the stator current and the rotor position. These inputs pass through the hidden layers. This data is then processed as flux linkage and torque outputs. The concept is illustrated in Fig. 14. The four-layer network consists of one input layer, two hidden layers and one output layer. The input layer has two tiers to take the stator current and rotor position. Each hidden layer consists of four tiers whereas the output layer has two tiers. Various neural networks can be identified based on the way of processing the data in each tier. Recurrent Neural Networks (RNN) [69] and Radial Basis Function (RBF) neural networks [74] are more popular in SRM modeling. The learning techniques are applied to train the neural networks. This is necessary such that the network functions properly. There are various learning techniques that have been applied in SRM modeling such as back-propagation algorithm [70], B-spline neural network [71], Cascade-Forward-backpropagation Neural Network (CFNN) [72], General Regression Neural Network (GRNN) [73], Fuzzy clustering [74], and hybrid Adaptive Neural Fuzzy Inference System (ANFIS) [75]. Artificial intelligence provides models with high accuracy but it requires large number of data points to train the network. The large data set requirement causes overfitting [76]; i.e. the accuracy of the fitted model is high within the given data set and low outside. ML techniques address this issue [76], [77]. They are developed based on the statistics theory [76]. The most popular ML technique in SRM modeling is the Least Square Support Vector Machine (LSSVM) technique [76], [77]. Grid-Diamond Search (GDS) algorithm is applied to optimize the machine model developed using LSSVM technique [77].

As a summary, the polynomial functions, exponential functions and Fourier series technique can provide higher accuracy for the flux linkage/inductance profiles of the SRM compared to FEM. In addition to that, ANN and ML techniques can also provide high accuracy in comparison with FEM. However, those techniques consume large amount of time to develop the learning mechanism.

IV. NUMERICAL MODELING TECHNIQUES OF SRMS

A. FINITE ELEMENT METHOD (FEM)

Among all numerical modeling techniques, FEM is considered as the most popular technique for modeling SRMs [28]. It is utilized in the design, analysis, and optimization of SRMs. The FEM is applied to design and analyze SRMs with various stator/rotor topologies [8], [78]–[81], stator/rotor segmented designs [78], double stator/rotor designs [81], and designs

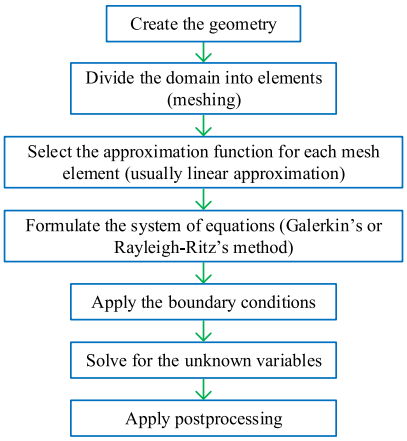

FIGURE 15. Procedure of the FE analysis.

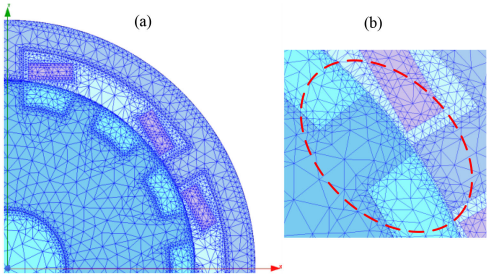

FIGURE 16. A mesh of a quarter model of a 6/14 SRM (a) whole mesh and (b) mesh near the airgap.

with multi-level airgaps [82]. It is also used in optimizing SRM designs to achieve different objectives such as to maximize the developed torque [8], [10], [78], minimize the torque ripple [9], [10], [79], minimize the Back EMF (BEMF) harmonics [80], minimize the machine weight and volume [80], [81], [83], and minimize the winding AC copper losses (DC copper loss and eddy current loss) [84], [85]. Despite the irregular flux pattern inside the machine slots, the FEM gives a relatively accurate calculation of the winding eddy-current density distribution [14].

The FE analysis procedure is shown in Fig. 15. The machine domain is discretized into a finite number of elements. A possible discretization of a quarter model of a 6/14 SRM is shown in Fig. 16(a). The accuracy of the FE model depends on the number of mesh elements [20]. SRMs operate in saturation conditions, so it is necessary to increase the number of elements in the highly saturated regions to improve the model accuracy. Moreover, the machine airgap is changing with the rotation of the rotor, so it requires a large number of elements. This can be seen in Fig. 16(b). Generally, magnetic vector potential or magnetic scalar potential are utilized to formulate the 2D FE system of equations [21]. The magnetic-vector-potential-based formulation is less suitable for 3D FE

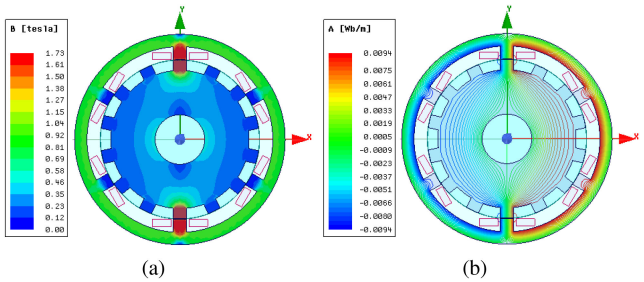

FIGURE 17. FE simulation model of a 6/14 SRM (a) Flux density distribution in the stator and rotor and (b) Flux lines inside the machine at aligned position.

problems since it makes the system more complex and increases the computation burden significantly [14]. The 2D FE problem can be formulated using magnetic vector potential.

A system of equations is developed for each element in terms of the magnetic vector potentials at the element nodes. These local systems are assembled together to formulate one global system of equations. Dirichlet, Neumann, and periodic boundary conditions are applied to the formulated system [20].

Due to the nonlinearity of the magnetic materials, the formulated system of equations is nonlinear. Numerical techniques, such as Newton-Raphson method, are used to solve for the magnetic vector potentials [86]. Post-processing is then applied to the converged magnetic vector potentials to calculate various electromagnetic quantities such as flux linkage, flux density, and electromagnetic torque. The flux density distribution and flux lines in the stator and rotor of a FE model of a 6/14 SRM is shown in Fig. 17.

B. BOUNDARY ELEMENT METHOD (BEM)

BEM is another technique to model SRMs. Boundary integral equations are used in BEM to solve the electromagnetic fields on the problem domain boundary. BEM has been applied in the design and optimization of SRMs [87]. The accuracy of the BEM is as high as the FEM, and it requires lower computational burden [88]. However, its major drawback is the difficulty of considering the magnetic saturation [21] due to non-symmetric and fully populated coefficient matrices. Therefore, BEM and FEM [88], [89] or BEM and MEC [90] are commonly combined together to model SRMs. The FEM or MEC estimates the magnetic fields in the nonlinear regions whereas the BEM solves the magnetic field in the linear regions. Solving the electromagnetic field in the nonlinear region using MEC instead of using FEM reduces the computational burden and increases the simulation speed.

Meshing in BEM is performed at the machine boundary. The boundary mesh elements are one-dimensional for 2D domain and two-dimensional for 3D domain [14]. That is why it is less complex compared to FEM. A possible boundary mesh of a 2D half model of an 8/6 SRM is shown in Fig. 18. The mesh can be further refined to increase the accuracy. As

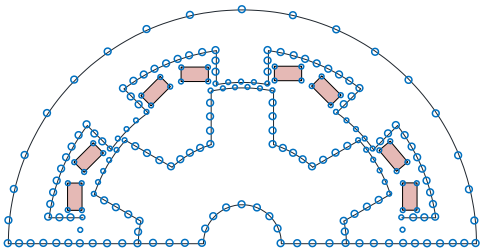

FIGURE 18. A boundary element mesh of a half model of an 8/6 SRM.

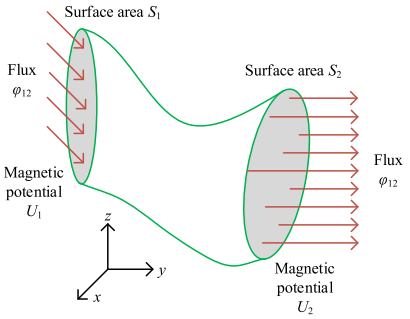

FIGURE 19. An arbitrary flux tube representation of flux path.

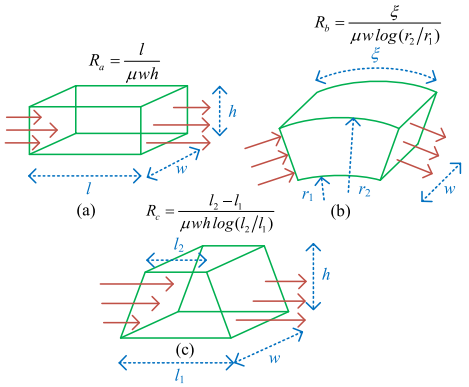

FIGURE 20. Common flux tube shapes for SRMs [26]:(a) rectangular shape, (b) curvilinear rectangular shape, and (c) trapezoidal shape elements.

in the FEM, a global coefficient matrix can be developed for BEM by assembling each local coefficient matrices. Hence the magnetic vector or scalar potential can be calculated inside the region of the boundary mesh region.

V. MEC MODELING TECHNIQUES OF SRMS

The MEC method became popular in modeling SRMs in the past decade [14], [91]. In this method, the SRM geometry is represented as a magnetic circuit, that is analogues to an electric circuit. Then, the flux distribution inside the machine is calculated by solving the magnetic circuit. After that, the flux density, magnetic field intensity, phase flux linkage, and electromagnetic torque can be determined. The MEC technique is usually utilized to provide preliminary designs [92]–[95] and to analyze the electromagnetic characteristics [91], [96], [97] of SRMs. This technique is divided into two approaches: conventional MEC approach [98]–[100] and reluctance-mesh/finite-reluctance approach (FRA) [101]–[104].

A. CONVENTIONAL MEC APPROACH

This approach is simpler and faster compared to FEM. However, it is necessary to define the flux paths inside the machine before the modeling. The approach is based on Hopkinson's law [103] which can be stated as

$$U = \phi R_{mag} \tag{10}$$

The magnetic scalar potential U across a reluctance element is obtained from [105]

$$U = \int_l \vec{H}.d\vec{l} \tag{11}$$

where l is the length of the reluctance element. The magnetic flux ϕ can be defined as [103]

$$\phi = \iint_S \vec{B}.d\vec{S} \tag{12}$$

where S is the surface area through which the flux passes. The magnetic reluctance is a function of the magnetic circuit geometry and material permeability. The concept of flux tube can be applied to evaluate the reluctance of different geometries. A flux tube is an arbitrary 3D tube-shaped volume where flux enters from one side, and leaves from the other side as shown in Fig. 19 [105]–[107]. A general expression of the reluctance R_{mag} of this arbitrary geometry is [106]

$$R_{mag} = \int_0^l \frac{dl}{\mu S(l)} \tag{13}$$

where l is the position along the flux tube length. Three common flux tube shapes could be utilized in an SRM as illustrated in Fig. 20 [108]. Applying (13), the corresponding reluctances in Fig. 20(a), (b) and (c) can be evaluated as

$$R_a = \int_0^l \frac{dl}{\mu\, w\, h} = \frac{l}{\mu\, w\, h} \tag{14}$$

$$R_b = \frac{\xi}{\mu\, w\, log(r_2/r_1)} \tag{15}$$

$$R_c \frac{l_2 - l_1}{\mu\, w\, h\, log(l_2/l_1)} \tag{16}$$

It is necessary to identify the flow paths of the flux inside the machine to develop the conventional MEC model. The identified flux paths can be divided into different flux tubes [92], [96], [97], [109], [110]. Each flux tube can be represented as a reluctance in the MEC model. A section of a developed conventional MEC model of the stator, rotor, and airgap of an SRM is shown in Fig. 21. The rotor is at the aligned position. The leakage fluxes between stator poles, and between stator poles and stator yoke are neglected. Three main reluctance types are considered in an SRM [111]. Linear reluctance for

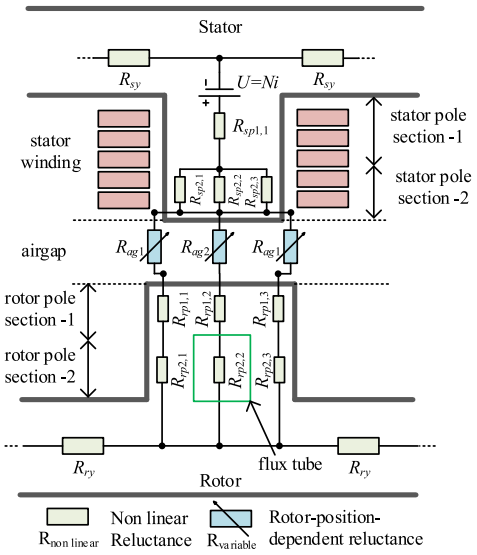

FIGURE 21. A conventional MEC of an SRM at the aligned position [98].

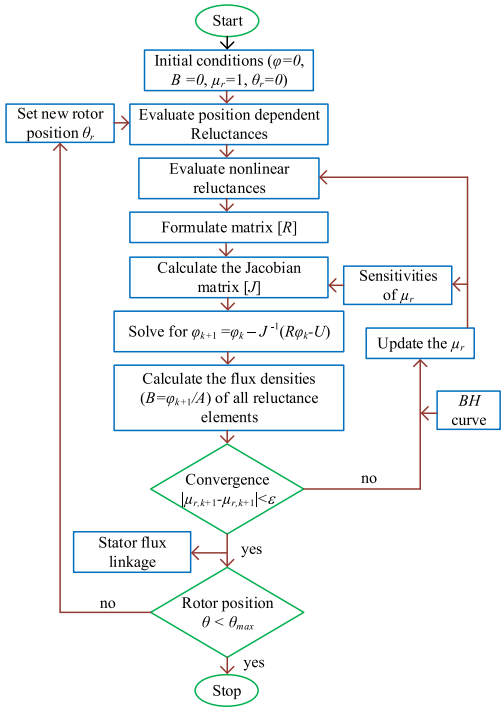

FIGURE 22. An example Newton-Raphson iterative method for solving the MEC model [101].

materials with constant permeability, nonlinear reluctance for materials with nonlinear *B-H* characteristics, and position-dependent reluctance that depends on the rotor position. The third type is used in the airgap and has a constant relative permeability of 1. As shown in Fig. 21, both stator and rotor poles are divided into two sections, designated as section-1 and section-2 for each pole. This division helps estimating the local saturation accurately. The top section of the stator pole, section-1, has a single reluctance element $R_{sp1,1}$ whereas the bottom section, section-2, has three reluctance elements, $R_{sp2,1}$, $R_{sp2,2}$, and $R_{sp2,3}$. The flux flow inside the rotor pole becomes nonuniform if the rotor pole moves away from the excited stator pole. Thus, more discretization is necessary in the rotor pole region to improve the model accuracy. In Fig. 21, the rotor pole is divided into two sections, and each section has three reluctance elements. Hence, the rotor pole has six reluctances which are $R_{rp1,1}$-$R_{rp1,3}$ and $R_{rp2,1}$-$R_{rp2,3}$. Both stator and rotor yokes are divided into two sections. Each stator and rotor yoke section has the same reluctances R_{sy} and R_{ry} since flux tubes in those sections have the same mean length and cross-section area. The airgap contains three reluctance elements. Two R_{ag1} reluctances corresponding to the fringing flux flowing through the non-overlap region between the stator and rotor poles. R_{ag2} corresponds to the flux passing through the overlap region. These airgap reluctances depend on the rotor position. The MMF source in the model represents the winding current times the number of turns N.

The mesh/nodal analysis techniques based on Kirchoff's laws can be applied to solve for the flux/magnetic potentials of each reluctance element in the circuit illustrated in Fig. 21 [101], [105]. The mesh analysis technique is the most common way to calculate the flux that flows through the reluctance elements. Flux loops are defined in the MEC model, where each loop contains various reluctance elements and MMF sources. The following matrix equation can be applied to obtain the flux in each flux loop.

$$[R]_{(n_{fl}\times n_{fl})}[\phi]_{(n_{fl}\times 1)} = [U]_{(n_{fl}\times 1)} \tag{17}$$

where $[\phi]$ and $[U]$ are vectors that include the fluxes and MMF sources, respectively. The parameter n_{fl} is the total number of flux loops in the magnetic circuit. Due to the nonlinearity of the stator and rotor reluctances, some elements in the matrix $[R]$ are functions of the flux density. Hence, (17) is nonlinear, and iterative techniques such as simple iterations [96], [110], Gauss-Seidal method [97], and Newton-Raphson method [101] are utilized to solve it. An iterative procedure with the Newton-Raphson method is shown in Fig. 22 as an example. The initial value of the rotor position and fluxes are set to zero. The initial values of the relative permeability μ_r is set to one and the initial flux density of any nonlinear reluctance is set to zero. The airgap reluctances are evaluated based on the rotor position whereas the nonlinear reluctances are evaluated based on the relative permeability. The matrix $[R]$ is then formulated, and the Newton-Raphson method is applied to calculate the loop fluxes. Then, the flux densities of the nonlinear reluctances are calculated. After that, the convergence criteria is checked. If it is not met, the relative permeabilities and, hence, the nonlinear reluctances are updated based on the calculated flux densities and the material *B-H* characteristic. This process then repeats until the convergence criteria is achieved. Once the process converges, the flux linkage is calculated at this particular rotor position. Similar calculations are repeated for different rotor positions.

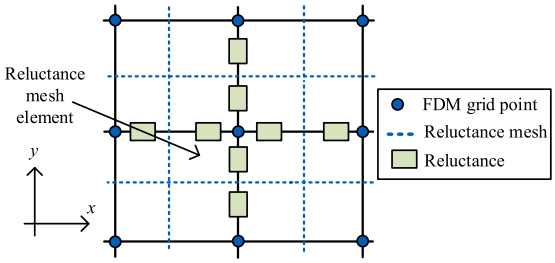

FIGURE 23. A general 2D section of a grid created in finite difference method.

The conventional MEC approach can be further extended to model the mutual coupling, multi-phase excitation [97], [99], and asymmetric airgap [109] in SRMs. The MEC models can be coupled with numerical or analytical models to develop hybrid models. In [112], [113], the airgap reluctances are obtained by FE simulations whereas the stator and rotor reluctances were modeled based on the conventional MEC approach. Instead of using FE simulations, analytical techniques may also be used to calculate the airgap reluctances, as in [114]. In [24], [25] and [115]–[117], analytical methods based on the MEC approach were proposed to estimate the phase flux linkage/phase inductance of an SRM. These methods are easy to implement and faster than solving the MEC numerically. However, leakage fluxes and local saturation in the stator and rotor poles were neglected in these analyses.

B. RELUCTANCE MESH/FINITE RELUCTANCE APPROACH

This approach can be considered as an extension of the Finite Difference Method. In FDM, the problem domain is divided into discrete grid points as shown in Fig. 23. Then, the partial derivatives of magnetic scalar potential in (5) are approximated using finite differences and the potential values on the grid points [23], [101], [102], [105]. In the reluctance mesh approach, the reluctances are defined between adjacent grid points as illustrated in Fig. 23 [14]. A reluctance mesh element, as depicted in Fig. 23, is defined around each grid point. The shape of the element is mainly rectangular, curvilinear rectangular, or trapezoidal as in Fig. 20. However, other shapes such as diamond [102] and hexagon [118] have also been utilized. Fig. 24 shows the 2D section of an open-profile SRM that is divided into a rectangular-shaped grid. The reluctance elements in the regions of stator slots are associated with currents produces by the stator winding. Therefore, those regions can be considered as non-current-free regions. The reluctance elements in the stator and rotor core do not have any currents associated with them if the eddy current effects are neglected. Therefore, reluctance elements in the stator and rotor regions can be considered as current-free regions. The airgap region can also be considered as a current-free region since there are no current carrying conductors in the airgap. A general reluctance element in the current-free region in the grid in Fig. 24 is shown in Fig. 25. The partial derivatives in (5) can be approximated by applying FDM for the element in

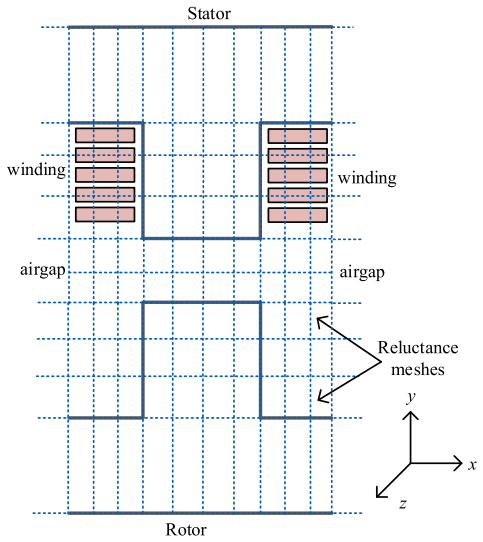

FIGURE 24. A reluctance mesh developed for an SRM.

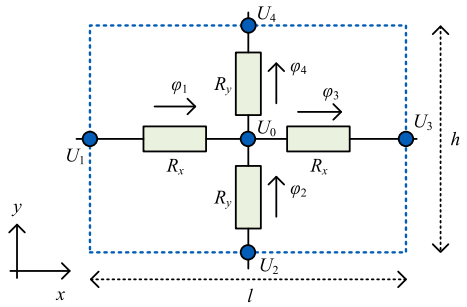

FIGURE 25. A reluctances mesh element in Fig. 24 in the current-free region [119].

Fig. 25 using magnetic scalar potential values U_1, U_2, U_3 and U_4, and dimensions l and h of the element [22], [120] as

$$\mu\left(\frac{U_1-U_0}{l^2}+\frac{U_3-U_0}{l^2}\right)+\mu\left(\frac{U_2-U_0}{h^2}+\frac{U_4-U_0}{h^2}\right)=0 \quad (18)$$

There are no electric vector potential terms in (18) since the reluctance element is in the current-free region. Equation (18) can be further simplified as

$$\frac{U_1-U_0}{R_x}+\frac{U_3-U_0}{R_x}+\frac{U_2-U_0}{R_y}+\frac{U_4-U_0}{R_y}=0 \quad (19)$$

where the reluctances R_x and R_y equal to $2l/(\mu\, w\, h)$ and $2h/(\mu\, w\, l)$, respectively. The variable w is the axial length of the machine.

A similar procedure can be applied to the grid elements in the stator-slot regions as shown in Fig. 26. Again, the partial derivatives in (5) can be approximated by applying FDM for

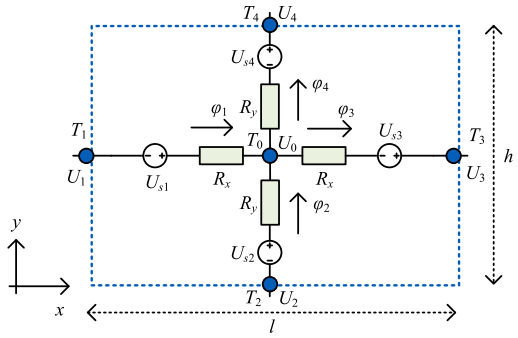

FIGURE 26. A reluctance mesh element in non-current-free region [119].

the element in Fig. 26 as

$$\mu\left(\frac{U_1-U_0}{l^2}+\frac{U_3-U_0}{l^2}\right)+\mu\left(\frac{U_2-U_0}{h^2}+\frac{U_4-U_0}{h^2}\right)$$
$$=\mu\left(\frac{T_1-T_0}{l}-\frac{T_3-T_0}{l}\right)+\mu\left(\frac{T_2-T_0}{h}-\frac{T_4-T_0}{h}\right) \quad (20)$$

where T_0, T_1, T_2, T_3 and T_4 are electric vector potentials of the nodes in Fig. 26, respectively. The terms with the electric vector potentials in (20) can be represented as lumped MMF sources as in Fig. 26 [104], [119]. The Ampere's law can be applied to determine the MMF distribution along x and y directions in stator slot regions [119]. Then, the MMF source along the x direction can be divided into two equal MMF sources placed at the left hand (U_{s1}) and right hand (U_{s3}) sides of the element as in Fig. 26. Similar, procedure can be applied to place the MMF sources at the top (U_{s4}) and bottom (U_{s2}) sides of the element. Then, equation (20) can be simplified as

$$\frac{U_1-U_0+U_{s1}}{R_x}+\frac{U_3-U_0-U_{s3}}{R_x}$$
$$+\frac{U_2-U_0+U_{s2}}{R_y}+\frac{U_4-U_0-U_{s4}}{R_y}=0 \quad (21)$$

where U_{s1}, U_{s2}, U_{s3}, and U_{s4} are the values of the MMF sources exist inside the reluctance mesh element.

Unlike the conventional MEC approach, in FDM the flux path inside the machine is not required to be known in advance to develop the reluctance mesh MEC model. The accuracy of the reluctance mesh model can be improved by refining the grid. However, this increases the number of elements and, hence, the computational burden and the simulation time. Additionally, the 2D reluctance elements in (19) and (21) can be extended to 3D by adding two additional reluctance elements along the z-axis [105]. As in the conventional MEC technique, (17) can be applied in reluctance mesh MEC technique to calculate the flux passing through each reluctance element.

VI. DISCUSSIONS, POTENTIAL RESEARCH DIRECTIONS AND RESEARCH AREAS

In this paper, we have investigated various modeling techniques for SRMs. Table 3 summarizes the advantages, disadvantages, and applications of these techniques. These models are compared in terms of the accuracy, computational time, and the capability of modeling local saturation, electromagnetic losses, complex geometries, and 3D effects. It can be concluded that proper selection of the modeling technique depends on the application, required accuracy, suitable simulation speed, and available computational power. The MEC techniques are becoming more popular among researchers due to their faster simulation speed and fair accuracy as compared to the FEM [14]. The saturation, leakage fluxes, and mutual coupling of SRMs can be modeled considering rotation of the rotor.

The challenges with the existing SRM modeling techniques can be overcome by utilizing hybrid modeling techniques [88], [89], [112]–[114]. For instance, the disadvantages of Maxwell's equation-based modeling technique and FEM can be minimized by combining both techniques. Furthermore, the design and operational challenges of SRM can be addressed by extending the existing modeling techniques or introducing new ones. For example, for acoustic noise analysis, which is a major challenge in SRMs, the radial forces in the airgap and their harmonic content need to be calculated. Accurate and computationally efficient modeling techniques are required to calculate the radial forces [121], [122]. Reluctance mesh technique, ANN, and ML-based techniques can be improved to calculate the radial forces. For modeling and design of axial flux SRMs, extensive and computationally efficient 3D magnetic models are necessary [5], [7]. The reluctance mesh technique or hybrid modeling techniques can be extended to model a 3D geometry to achieve higher accuracy and computational speed. Based on the previous discussions in this study, the following potential research areas are proposed.

A. RELUCTANCE MESH APPROACH

The key advantage of the reluctance mesh approach over the conventional MEC technique is that it does not require an advanced knowledge of the flux path inside the machine [97]. This technique has been widely used to model and analyze PM machines [101], [102]. This is not the case for SRMs. Studying the reluctance mesh approach for different SRM configurations is a potential research field. Another potential area is using this technique to model the effect of mutual coupling on the dynamic performance of SRMs.

B. MODELING OF THE ELECTROMAGNETIC LOSSES IN SRMS

Analytical models are not capable of calculating the electromagnetic losses in SRMs accurately such as hysteresis losses, eddy-current losses, and AC copper losses. According to the available literature, the FEM is the most applied technique to estimate the motor losses [84], [85]. However, the reluctance

TABLE 3. Comparison of Electromagnetic Modeling Techniques for SRMs

Model		Advantages	Disadvantages	Applications
Analytical	Maxwell's equations	Low computation time; easy to develop	Difficult to model local saturation, complex geometries, 3D effects and electromagnetic losses	Electromagnetic analysis & preliminary design
	Interpolation & curve fitting	Low computation time, easy to develop, can include local saturation	New data is required if the machine geometry changes	Motor drives
Numerical	FEM	High accuracy; can model complex geometries, 3D effects, electromagnetic losses, local saturation; the matrix assembly is simple	Requires large computation time and memory	Electromagnetic design & analysis, optimization
	BEM	High accuracy; can model complex geometries, 3D effects; requires moderate computational time and memory	Difficult to model local saturation, electromagnetic losses; matrix assembly is difficult	Electromagnetic design & analysis, optimization (Combined with FEM/MEC)
MEC	Conventional	Easy to develop; low computation time; can model local saturation electromagnetic losses; matrix assembly is simple	Difficult to model complex geometries, 3D effects; has moderate accuracy; requires defining flux paths in advance	Electromagnetic design & analysis
	Reluctance Mesh	Good accuracy; can model complex geometries, 3D effects, local saturation, electromagnetic losses; does not require defining flux path in advance; matrix assembly is easy	Requires moderate computational time and memory	Electromagnetic design & analysis, optimization

mesh technique is a potential alternative. Various techniques such as Preisach model [101], Jile-Atherton model [123], and the concept of magnetic inductance [124] were coupled with the MEC technique to model the hysteresis losses in induction machines and SRMs. However, to the best of authors' knowledge, these models were not coupled with the reluctance mesh approach. In the literature, the concept of magnetic capacitance [119] was coupled with the reluctance mesh approach to estimate the eddy current losses in an induction machine. But, no references were found discussing how to apply this method to SRMs.

C. CALCULATION OF THE AIRGAP RADIAL AND TANGENTIAL FORCES

The airgap radial and tangential forces are necessary to analyze the acoustic noise and vibration characteristics, and electromagnetic torque. The conventional MEC technique has been applied to calculate the radial forces in the airgap of an SRM [109]. However, to the best of authors' knowledge, the reluctance mesh technique has not been utilized to estimate these forces. The radial and tangential components of the airgap magnetic flux density can be estimated using the reluctance mesh technique. Then, Maxwell Stress Tensor can be applied to calculate the radial and tangential forces densities.

D. HYBRID MODELING TECHNIQUES OF SRMS

Hybrid modeling techniques has become more popular recently since the advantages are exploited by combining different techniques. FEM has been hybridized with MEC in [112] and [113], and with BEM in [88] and [89] to reduce the computational burden. In addition, analytical models have been combined with the conventional MEC models such as in [114]. There is a potential to combine any of the MEC approaches with the BEM to model SRMs. The BEM can be utilized to model the airgap field whereas the MEC approach can model the iron core as it can consider the effect of local saturation.

VII. CONCLUSION

This paper presents various modeling techniques for Switched Reluctance Motor Drives. Analytical as well as numerical techniques have been considered. The analytical techniques are based on either Maxwell's equations or interpolation and curve fitting methods. Maxwell's-equations-based analytical models are fast and computationally inexpensive. However, they are not accurate enough due to the applied assumptions and approximations, and the difficulty in modeling nonlinearity due to the saturation of the magnetic core. However, the accuracy could be improved by coupling the analytical models with interpolation and curve fitting methods using finite element or experimental data.

The numerical techniques are the most popular modeling approach for electric machines due to their high accuracy. The FEM is the most common method for SRM modeling. However, it is computationally expensive and requires a longer simulation time compared to analytical methods. The BEM is another numerical approach to model SRMs. It has comparable accuracy with respect to FEM and it has lower computational burden. However, its major drawback is the difficulty in considering the magnetic saturation.

The MEC technique can alternatively be utilized for modeling SRMs. This technique has higher accuracy as compared to analytical models and it is faster and computationally inexpensive compared to the FEM. The MEC techniques can be divided into two main categories, (i) conventional MEC approach and (ii) reluctance mesh/finite reluctance approach. In the conventional MEC, it is required to know the flux path inside the machine in advance. But, this is not the case in the reluctance mesh approach. Conventional MEC technique

takes less computational time and reluctance mesh technique takes moderate computational time.

Finally, the paper summarizes the advantages, disadvantages, and applications of the various modeling techniques of SRMs. It also proposes potential research directions and areas to be considered. The Maxwell's equation based SRM models and MEC based SRM models are suitable for initial sizing of SRMs. The interpolation- and curve-fitting based methods can be used for controller design of SRM drives. The FEM and BEM based SRM models are useful for designing and optimizing the SRMs.

ACKNOWLEDGMENT

The authors would like to thank ANSYS, and Mathworks for their support with Maxwell, and MATLAB software in this research.

REFERENCES

[1] B. Bilgin, J. W. Jiang, and A. Emadi, *Switched Reluctance Motor Drives: Fundamentals to Applications*. Boca Raton, FL, USA: CRC Press, 2019.

[2] L. Maharjan *et al.*, "Comprehensive report on design and development of a 100-kW DSSRM," *IEEE Trans. Transp. Electrific.*, vol. 4, no. 4, pp. 835–856, Dec. 2018.

[3] C. Gan, J. Wu, Q. Sun, W. Kong, H. Li, and Y. Hu, "A review on machine topologies and control techniques for low-noise switched reluctance motors in electric vehicle applications," *IEEE Access*, vol. 6, pp. 31 430–31 443, May 2018.

[4] A. Labak and N. C. Kar, "Designing and prototyping a novel five-phase pancake-shaped axial-flux SRM for electric vehicle application through dynamic FEA incorporating flux-tube modeling," *IEEE Trans. Ind. Appl.*, vol. 49, no. 3, pp. 1276–1288, Jun. 2013.

[5] H. Arihara and K. Akatsu, "Basic properties of an axial-type switched reluctance motor," *IEEE Trans. Ind. Appl.*, vol. 49, no. 1, pp. 59–65, Feb. 2012.

[6] R. Madhavan and B. G. Fernandes, "Axial flux segmented SRM with a higher number of rotor segments for electric vehicles," *IEEE Trans. Energy Convers.*, vol. 28, no. 1, pp. 203–213, Mar. 2013.

[7] T. Shibamoto, K. Nakamura, H. Goto, and O. Ichinokura, "A design of axial-gap switched reluctance motor for in-wheel direct-drive EV," in *Proc. IEEE Int. Conf. Elect. Mach.*, Sep. 2012, pp. 1160–1165.

[8] S. R. Mousavi-Aghdam, M. R. Feyzi, N. Bianchi, and M. Morandin, "Design and analysis of a novel high-torque stator-segmented SRM," *IEEE Trans. Ind. Electron.*, vol. 63, no. 3, pp. 1458–1466, Mar. 2015.

[9] H. Chen, W. Yan, J. J. Gu, and M. Sun, "Multiobjective optimization design of a switched reluctance motor for low-speed electric vehicles with a Taguchi–CSO algorithm," *IEEE/ASME Trans. Mechatronics*, vol. 23, no. 4, pp. 1762–1774, Aug. 2018.

[10] C. Ma and L. Qu, "Multiobjective optimization of switched reluctance motors based on design of experiments and particle swarm optimization," *IEEE Trans. Energy Convers.*, vol. 30, no. 3, pp. 1144–1153, Sep. 2015.

[11] B. Fahimi, A. Emadi, and R. B. Sepe, "Four-quadrant position sensorless control in SRM drives over the entire speed range," *IEEE Trans. Power Electron.*, vol. 20, no. 1, pp. 154–163, Jan. 2005.

[12] X. Xue *et al.*, "Optimal control method of motoring operation for SRM drives in electric vehicles," *IEEE Trans. Veh. Technol.*, vol. 59, no. 3, pp. 1191–1204, Mar. 2010.

[13] M. Yilmaz and P. T. Krein, "Capabilities of finite element analysis and magnetic equivalent circuits for electrical machine analysis and design," in *Proc. IEEE Power Electron. Specialists Conf.*, Jun. 2008, pp. 4027–4033.

[14] S. Li, S. Zhang, T. G. Habetler, and R. G. Harley, "Modeling, design optimization, and applications of switched reluctance machines–A review," *IEEE Trans. Ind. Appl.*, vol. 55, no. 3, pp. 2660–2681, Jun. 2019.

[15] Y. Zhang, K. Chau, J. Jiang, D. Zhang, and C. Liu, "A finite element–analytical method for electromagnetic field analysis of electric machines with free rotation," *IEEE Trans. Magn.*, vol. 42, no. 10, pp. 3392–3394, Oct. 2006.

[16] T. Lubin, H. Razik, and A. Rezzoug, "Magnetic saturation effects on the control of a synchronous reluctance machine," *IEEE Trans. Energy Convers.*, vol. 17, no. 3, pp. 356–362, Sep. 2002.

[17] G. Dajaku and D. Gerling, "Stator slotting effect on the magnetic field distribution of salient pole synchronous permanent-magnet machines," *IEEE Trans. Magn.*, vol. 46, no. 9, pp. 3676–3683, Sep. 2010.

[18] D. Wang, D. Zhang, X. Du, and X. Wang, "Unitized design methodology of linear switched reluctance motor with segmental secondary for long rail propulsion application," *IEEE Trans. Ind. Electron.*, vol. 65, no. 12, pp. 9884–9894, Dec. 2018.

[19] W. Uddin, T. Husain, Y. Sozer, and I. Husain, "Design methodology of a switched reluctance machine for off-road vehicle applications," *IEEE Trans. Ind. Appl.*, vol. 52, no. 3, pp. 2138–2147, Jun. 2016.

[20] N. Bianchi, *Electrical Machine Analysis Using Finite Elements*. Boca Raton, FL, USA: CRC Press, 2005.

[21] K. Hameyer and R. Belmans, *Numerical Modelling and Design of Electrical Machines and Devices*. Southampton, Boston: WIT Press, vol. 1, 1999.

[22] J. Sykulski, *Computational Magnetics*. Berlin, Germany: Springer, 1995.

[23] A. Demenko and J. K. Sykulski, "Analogies between finite-difference and finite-element methods for scalar and vector potential formulations in magnetic field calculations," *IEEE Trans. Magn.*, vol. 52, no. 6, Jun. 2016, Art. no. 7004206.

[24] W. Uddin and Y. Sozer, "Analytical modeling of mutually coupled switched reluctance machines under saturation based on design geometry," *IEEE Trans. Ind. Appl.*, vol. 53, no. 5, pp. 4431–4440, Oct. 2017.

[25] A. Radun, "Analytically computing the flux linked by a switched reluctance motor phase when the stator and rotor poles overlap," *IEEE Trans. Magn.*, vol. 36, no. 4, pp. 1996–2003, Jul. 2000.

[26] V. Ostovic, *Dynamics of Saturated Electric Machines*. New York, NY, USA: Springer, 2012.

[27] K. Vijayakumar, R. Karthikeyan, S. Paramasivam, R. Arumugam, and K. Srinivas,"Switched reluctance motor modeling, design, simulation, and analysis: A comprehensive review," *IEEE Trans. Magn.*, vol. 44, no. 12, pp. 4605–4617, Dec. 2008.

[28] E. Bostanci, M. Moallem, A. Parsapour, and B. Fahimi, "Opportunities and challenges of switched reluctance motor drives for electric propulsion: A comparative study," *IEEE Trans. Transp. Electrific.*, vol. 3, no. 1, pp. 58–75, Mar. 2017.

[29] A. Kladas and J. Tegopoulos, "A new scalar potential formulation for 3-d magnetostatics necessitating no source field calculation," *IEEE Trans. Magn.*, vol. 28, no. 2, pp. 1103–1106, Mar. 1992.

[30] A. Radun, "Analytical calculation of the switched reluctance motor's unaligned inductance," *IEEE Trans. Magn.*, vol. 35, no. 6, pp. 4473–4481, Nov. 1999.

[31] S. Li, S. Zhang, C. Gong, T. G. Habetler, and R. G. Harley, "An enhanced analytical calculation of the phase inductance of switched reluctance machines," *IEEE Trans. Ind. Appl.*, vol. 55, no. 2, pp. 1392–1407, Apr. 2018.

[32] M. Golzarzadeh and B. Ganji, "Analytical modelling of the linear switched reluctance motor with segmental translator," *IET Elect. Power Appl.*, vol. 13, no. 4, pp. 527–537, Apr. 2019.

[33] T. C. O'Connell and P. T. Krein, "A Schwarz–Christoffel-based analytical method for electric machine field analysis," *IEEE Trans. Energy Convers.*, vol. 24, no. 3, pp. 565–577, Sep. 2009.

[34] E. Ilhan, M. F. Kremers, E. T. Motoasca, J. J. Paulides, and E. A. Lomonova, "Spatial discretization methods for air gap permeance calculations in double salient traction motors," *IEEE Trans. Ind. Appl.*, vol. 48, no. 6, pp. 2165–2172, Dec. 2012.

[35] Z. Djelloul-Khedda, K. Boughrara, F. Dubas, and R. Ibtiouen, "Nonlinear analytical prediction of magnetic field and electromagnetic performances in switched reluctance machines," *IEEE Trans. Magn.*, vol. 53, no. 7, pp. 1–11, Jul. 2017.

[36] S. Li, S. Zhang, J. Dang, T. G. Habetler, and R. G. Harley, "Calculating the unsaturated inductance of 4/2 switched reluctance motors at arbitrary rotor positions based on partial differential equations of magnetic potentials," in *Proc. IEEE North Amer. Power Symp.*, Charlotte, NC, USA, Nov. 2015, pp. 1–8.

[37] Z. Poming, M. Qishuang, and X. Ping, "Modeling and analysis of switched reluctance machines using an improved conformal mapping method," in *Proc. IEEE Int. Conf. Elect. Mach. Syst.*, Harbin, China, Aug. 2019, pp. 1–4.

[38] S. Zhao, N. Cheung, C. Lee, X. Yang, and Z. Sun, "Survey of modeling methods for flux linkage of switched reluctance motor," in *Proc. IEEE Int. Conf. Power Electron. Syst. Appl.*, Jun. 2011, pp. 1–4.

[39] J. Pan, N. C. Cheung, and J. Yang, "High-precision position control of a novel planar switched reluctance motor," *IEEE Trans. Ind. Electron.*, vol. 52, no. 6, pp. 1644–1652, Dec. 2005.

[40] P. Chancharoensook and M. F. Rahman, "Dynamic modeling of a four-phase 8/6 switched reluctance motor using current and torque look-up tables," in *Proc. IEEE Ann. Conf. Ind. Electron. Soc. IECON*, Sevilla, Spain, Nov. 2002, vol. 1, pp. 491–496.

[41] K. M. Rahman and S. E. Schulz, "High-performance fully digital switched reluctance motor controller for vehicle propulsion," *IEEE Trans. Ind. Appl.*, vol. 38, no. 4, pp. 1062–1071, Aug. 2002.

[42] R. B. Inderka and R. W. De Doncker, "Ditc-direct instantaneous torque control of switched reluctance drives," *IEEE Trans. Ind. Appl.*, vol. 39, no. 4, pp. 1046–1051, Aug. 2003.

[43] P. Zhang, P. A. Cassani, and S. S. Williamson, "An accurate inductance profile measurement technique for switched reluctance machines," *IEEE Trans. Ind. Electron.*, vol. 57, no. 9, pp. 2972–2979, Sep. 2010.

[44] Z. Zhihui and L. Yuren, "Numerical and analytical modeling of switched reluctance machines," *J. Comput.*, vol. 7, no. 12, pp. 3036–3043, Dec. 2012.

[45] Y. Yang and A. Emadi, "Coupled switched reluctance machine modeling and simulations," in *Proc. IEEE Conf. Exp. Transp. Electrific. Asia-Pacific (ITEC Asia-Pacific)*, Beijing, China, Sep. 2014, pp. 1–6.

[46] J. Dong *et al.*, "Advanced dynamic modeling of three-phase mutually coupled switched reluctance machine," *IEEE Trans. Energy Convers.*, vol. 33, no. 1, pp. 146–154, Mar. 2017.

[47] O. Safdarzadeh, A. Mahmoudi, E. Afjei, and H. Torkaman, "Rotary-linear switched reluctance motor: Analytical and finite-element modeling," *IEEE Trans. Magn.*, vol. 55, no. 5, May 2019, Art. no. 8200710.

[48] G. S. Buja and M. I. Valla, "Control characteristics of the SRM drives. I. Operation in the linear region," *IEEE Trans. Ind. Electron.*, vol. 38, no. 5, pp. 313–321, Oct. 1991.

[49] M. Hassanin, M. T. Alrifai, and D. A. Torrey, "Experimentally verified flux density models for the switched-reluctance machine," *IEEE Trans. Magn.*, vol. 37, no. 5, pp. 3818–3824, Sep. 2001.

[50] M. Stiebler and K. Liu, "An analytical model of switched reluctance machines," *IEEE Trans. Energy Convers.*, vol. 14, no. 4, pp. 1100–1107, Dec. 1999.

[51] T. Miller and M. McGilp, "Nonlinear theory of the switched reluctance motor for rapid computer-aided design," *Proc. IEE B (Electric Power Appl.)*, vol. 137, no. 6, pp. 337–347, Nov. 1990.

[52] C. Roux and M. M. Morcos, "On the use of a simplified model for switched reluctance motors," *IEEE Trans. Energy Convers.*, vol. 17, no. 3, pp. 400–405, Sep. 2002.

[53] X. Xue, K. Cheng, and S. Ho, "A self-training numerical method to calculate the magnetic characteristics for switched reluctance motor drives," *IEEE Trans. Magn.*, vol. 40, no. 2, pp. 734–737, Mar. 2004.

[54] X.-D. Xue, K. Cheng, and S. Ho, "Simulation of switched reluctance motor drives using two-dimensional bicubic spline," *IEEE Trans. Energy Convers.*, vol. 17, no. 4, pp. 471–477, Dec. 2002.

[55] V. Nasirian, S. Kaboli, A. Davoudi, and S. Moayedi, "High-fidelity magnetic characterization and analytical model development for switched reluctance machines," *IEEE Trans. Magn.*, vol. 49, no. 4, pp. 1505–1515, Apr. 2012.

[56] H.-J. Chen, D.-Q. Jiang, J. Yang, and L.-X. Shi, "A new analytical model for switched reluctance motors," *IEEE Trans. Magn.*, vol. 45, no. 8, pp. 3107–3113, Aug. 2009.

[57] M. Farshad, J. Faiz, and C. Lucas, "Development of analytical models of switched reluctance motor in two-phase excitation mode: Extended miller model," *IEEE Trans. Magn.*, vol. 41, no. 6, pp. 2145–2155, Jun. 2005.

[58] D. Torrey and J. Lang, "Modelling a nonlinear variable-reluctance motor drive," *IEE Proc. B (Electric Power Appl.)*, vol. 137, no. 5, pp. 314–326, Sep. 1990.

[59] S. Mir, I. Husain, and M. E. Elbuluk, "Switched reluctance motor modeling with on-line parameter identification," *IEEE Trans. Ind. Appl.*, vol. 34, no. 4, pp. 776–783, Aug. 1998.

[60] S. A. Hossain and I. Husain, "A geometry based simplified analytical model of switched reluctance machines for real-time controller implementation," *IEEE Trans. Power Electron.*, vol. 18, no. 6, pp. 1384–1389, Nov. 2003.

[61] D. Essah and S. Sudhoff, "An improved analytical model for the switched reluctance motor," *IEEE Trans. Energy Convers.*, vol. 18, no. 3, pp. 349–356, Sep. 2003.

[62] X. Xue, K. Cheng, S. Ho, and K. Kwok, "Trigonometry-based numerical method to compute nonlinear magnetic characteristics in switched reluctance motors," *IEEE Trans. Magn.*, vol. 43, no. 4, pp. 1845–1848, Apr. 2007.

[63] C. S. Edrington, B. Fahimi, and M. Krishnamurthy, "An autocalibrating inductance model for switched reluctance motor drives," *IEEE Trans. Ind. Electron.*, vol. 54, no. 4, pp. 2165–2173, Aug. 2007.

[64] C. Yoopakdee and N. H. Fuengwarodsakul, "Analytic model of switched reluctance machine using combined fourier-polynomial approximation technique," in *Proc. IEEE Int. Conf. Elect. Mach.*, Alexandroupoli, Greece, Sep. 2018, pp. 1381–1387.

[65] F. R. Salmasi and B. Fahimi, "Modeling switched-reluctance machines by decomposition of double magnetic saliencies," *IEEE Trans. Magn.*, vol. 40, no. 3, pp. 1556–1561, May 2004.

[66] A. Khalil and I. Husain, "A Fourier series generalized geometry-based analytical model of switched reluctance machines," *IEEE Trans. Ind. Appl.*, vol. 43, no. 3, pp. 673–684, Jun. 2007.

[67] C. Lin, W. Wang, M. McDonough, and B. Fahimi, "An extended field reconstruction method for modeling of switched reluctance machines," *IEEE Trans. Magn.*, vol. 48, no. 2, pp. 1051–1054, Feb. 2012.

[68] S. Song, M. Zhang, and L. Ge, "A new decoupled analytical modeling method for switched reluctance machine," *IEEE Trans. Magn.*, vol. 51, no. 3, Mar. 2015, Art. no. 8100504.

[69] W. Lu, A. Keyhani, and A. Fardoun, "Neural network-based modeling and parameter identification of switched reluctance motors," *IEEE Trans. Energy Convers.*, vol. 18, no. 2, pp. 284–290, Jun. 2003.

[70] O. Ustun, "Measurement and real-time modeling of inductance and flux linkage in switched reluctance motors," *IEEE Trans. Magn.*, vol. 45, no. 12, pp. 5376–5382, Dec. 2009.

[71] Z. Lin, D. S. Reay, B. W. Williams, and X. He, "Online modeling for switched reluctance motors using B-spline neural networks," *IEEE Trans. Ind. Electron.*, vol. 54, no. 6, pp. 3317–3322, Dec. 2007.

[72] G.-Z. Cao, N. Chen, S.-D. Huang, S.-S. Xiao, and J. He, "Nonlinear modeling of the flux linkage in 2-D plane for the planar switched reluctance motor," *IEEE Trans. Magn.*, vol. 54, no. 11, Nov. 2018, Art. no. 8205805.

[73] H. Sahraoui, H. Zeroug, and H. Toliyat, "Switched reluctance motor design using neural-network method with static finite-element simulation," *IEEE Trans. Magn.*, vol. 43, no. 12, pp. 4089–4095, Dec. 2007.

[74] S. Zhou, "Modeling of switched reluctance motor based on combined clustering rbf network," in *Proc. IEEE Int. Conf. Elect. Mach. Syst.*, Sydney, NSW, Australia, Aug. 2017, pp. 1–5.

[75] W. Ding and D. Liang, "Modeling of a 6/4 switched reluctance motor using adaptive neural fuzzy inference system," *IEEE Trans. Magn.*, vol. 44, no. 7, pp. 1796–1804, Jul. 2008.

[76] S.-D. Huang, G.-Z. Cao, Z.-Y. He, J. Pan, J.-A. Duan, and Q.-Q. Qian, "Nonlinear modeling of the inverse force function for the planar switched reluctance motor using sparse least squares support vector machines," *IEEE Trans. Ind. Informat.*, vol. 11, no. 3, pp. 591–600, Jun. 2015.

[77] H. Likun, Y. Qingxin, and A. Jinlong, "Modeling of SRM based on XS-LSSVR optimized by GDS," *IEEE Trans. Appl. Supercond.*, vol. 20, no. 3, pp. 1102–1105, Jun. 2010.

[78] J. Y. Loh, M. A. Prabhu, S. Wang, S. C. Joshi, V. Viswanathan, and S. Ramakrishna, "Optimal segmented rotor design for the embedded electrical machine for the more electric aircraft," *J. Eng.*, vol. 2019, no. 17, pp. 4321–4324, Jun. 2019.

[79] J. W. Jiang, B. Bilgin, and A. Emadi, "Three-phase 24/16 switched reluctance machine for a hybrid electric powertrain," *IEEE Trans. Transp. Electrific.*, vol. 3, no. 1, pp. 76–85, Mar. 2017.

[80] A. A. S. Bukhari *et al.*, "Switched reluctance motor design for electric vehicles based on harmonics and back emf analysis," *J. Eng.*, vol. 2019, no. 17, pp. 4220–4225, Jun. 2019.

[81] Y. Yang, N. Schofield, and A. Emadi, "Double-rotor switched reluctance machine (DRSRM)," *IEEE Trans. Energy Convers.*, vol. 30, no. 2, pp. 671–680, Jun. 2015.

[82] J. Lin, T. Lambert, Y. Yang, B. Bilgin, R. Lankin, and A. Emadi, "A novel axial flux switched reluctance motor with multi-level air gap geometry," in *Proc. IEEE Elect. Power Energy Conf.*, Ottawa, ON, Canada, Oct. 2016, pp. 1–8.

[83] V. Rallabandi, J. Wu, P. Zhou, D. G. Dorrell, and D. M. Ionel, "Optimal design of a switched reluctance motor with magnetically disconnected rotor modules using a design of experiments differential evolution fea-based method," *IEEE Trans. Magn.*, vol. 54, no. 11, Nov. 2018, Art. no. 8205705.

[84] M. Klauz and D. G. Dorrell, "Eddy current effects in a switched reluctance motor," *IEEE Trans. Magn.*, vol. 42, no. 10, pp. 3437–3439, Oct. 2006.

[85] M. Al Eit, P. Dular, F. Bouillault, C. Marchand, and G. Krebs, "Perturbation finite element method for efficient copper losses calculation in switched reluctance machines," *IEEE Trans. Magn.*, vol. 53, no. 6, Jun. 2017, Art. no. 7202004.

[86] S. J. Salon, *Finite Element Analysis of Electrical Machines*. Norwell, MA, USA: Kluwer, 1995, vol. 101.

[87] Y. Tang and J. A. Kline, "Modeling and design optimization of switched reluctance machine by boundary element analysis and simulation," *IEEE Trans. Energy Convers.*, vol. 11, no. 4, pp. 673–680, Dec. 1996.

[88] T. C. O'Connell and P. T. Krein, "A time-harmonic three-dimensional vector boundary element model for electromechanical devices," *IEEE Trans. Energy Convers.*, vol. 25, no. 3, pp. 606–618, Sep. 2010.

[89] A. M. Omekanda, C. Broche, and M. Renglet, "Calculation of the electromagnetic parameters of a switched reluctance motor using an improved FEM-BIEM-application to different models for the torque calculation," *IEEE Trans. Ind. Appl.*, vol. 33, no. 4, pp. 914–918, Aug. 1997.

[90] D. M. Araujo, J.-L. Coulomb, O. Chadebec, and L. Rondot, "A hybrid boundary element method-reluctance network method for open boundary 3-D nonlinear problems," *IEEE Trans. Magn.*, vol. 50, no. 2, pp. 77–80, Feb. 2014.

[91] T. A. Lipo, *Introduction to AC Machine Design*. Hoboken, NJ, USA: Wiley, 2017.

[92] W. Ding, Z. Yin, L. Liu, J. Lou, Y. Hu, and Y. Liu, "Magnetic circuit model and finite-element analysis of a modular switched reluctance machine with e-core stators and multi-layer common rotors," *IET Electric Power Appl.*, vol. 8, no. 8, pp. 296–309, Sep. 2014.

[93] A. Labak and N. C. Kar, "Designing and prototyping a novel five-phase pancake-shaped axial-flux SRM for electric vehicle application through dynamic FEA incorporating flux-tube modeling," *IEEE Trans. Ind. Appl.*, vol. 49, no. 3, pp. 1276–1288, Jun. 2013.

[94] L.-L. Zhu, D. Xu, Q. Li, W. Sun, and Y.-Q. Hu, "Analysis and optimization of equivalent magnetic circuit model for a hybrid axial field flux-switching permanent magnet machine," in *Proc. IEEE Int. Conf. Elect. Mach. Syst.*, Oct. 2018, pp. 407–412.

[95] J. Ma, R. Qu, and J. Li, "Optimal design of axial flux switched reluctance motor for electric vehicle application," in *Proc. IEEE Int. Conf. Elect. Mach. Syst.*, Hangzhou, China, Oct. 2014, pp. 1860–1865.

[96] S. Yavuz, N. Parspour, and L. Ma, "Analytical modelling of a parametrized switched reluctance motor with adapting flux tube method," in *Proc. IEEE Int. Conf. Ind. Tech.*, Lyon, France, Feb. 2018, pp. 335–340.

[97] A. Deihimi, S. Farhangi, and G. Henneberger, "A general nonlinear model of switched reluctance motor with mutual coupling and multiphase excitation," *Elect. Eng.*, vol. 84, no. 3, pp. 143–158, Dec. 2002.

[98] M. Preston and J. Lyons, "A switched reluctance motor model with mutual coupling and multi-phase excitation," *IEEE Trans. Magn.*, vol. 27, no. 6, pp. 5423–5425, Nov. 1991.

[99] J. M. Kokernak and D. A. Torrey, "Magnetic circuit model for the mutually coupled switched-reluctance machine," *IEEE Trans. Magn.*, vol. 36, no. 2, pp. 500–507, Mar. 2000.

[100] Y. Tang, J. J. Paulides, and E. A. Lomonova, "Automated design of dc-excited flux-switching in-wheel motor using magnetic equivalent circuits," *IEEE Trans. Magn.*, vol. 51, no. 4, Mar. 2015, Art. no. 8103411.

[101] N. Li, J. Zhu, M. Lin, G. Yang, Y. Kong, and L. Hao, "Analysis of axial field flux-switching memory machine based on 3-D magnetic equivalent circuit network considering magnetic hysteresis," *IEEE Trans. Magn.*, vol. 55, no. 6, Jun. 2019, Art. no. 7203104.

[102] D. Cao, W. Zhao, J. Ji, L. Ding, and J. Zheng, "A generalized equivalent magnetic network modeling method for vehicular dual-permanent-magnet vernier machines," *IEEE Trans. Energy Convers.*, vol. 34, no. 4, pp. 1950–1962, Dec. 2019.

[103] C. Bruzzese, D. Zito, and A. Tessarolo, "Finite reluctance approach: A systematic method for the construction of magnetic network-based dynamic models of electrical machines," in *Proc. IEEE Ann. Conf. From Res. Ind.: Need More Effective Tech. Transfer*, Trieste, Italy, Sep. 2014, pp. 1–6.

[104] H. Xie, G. Krebs, M. H. Hassan, M. Zhang, C. Marchand, and Z. Ren, "A new reluctance network-based method with complementary distributed magnetomotive forces," *IEEE Trans. Magn.*, vol. 55, no. 6, Jun. 2019, Art. no. 8103805.

[105] M. Amrhein and P. T. Krein, "3-D magnetic equivalent circuit framework for modeling electromechanical devices," *IEEE Trans. Energy Convers.*, vol. 24, no. 2, pp. 397–405, Jun. 2009.

[106] H. Chen, W. Yan, and Z. Li, "Flux characteristics analysis of a single-phase tubular switched reluctance linear launcher," *IEEE Trans. Plasma Sci.*, vol. 47, no. 5, pp. 2316–2322, May 2019.

[107] A. Stuikys and J. K. Sykulski, "An efficient design optimization framework for nonlinear switched reluctance machines," *IEEE Trans. Ind. Appl.*, vol. 53, no. 3, pp. 1985–1993, Jun. 2017.

[108] B. du Peloux, L. Gerbaud, F. Wurtz, V. Leconte, and F. Dorschner, "Automatic generation of sizing static models based on reluctance networks for the optimization of electromagnetic devices," *IEEE Trans. Magn.*, vol. 42, no. 4, pp. 715–718, Apr. 2006.

[109] H. Chen and W. Yan, "Flux characteristics analysis of a double-sided switched reluctance linear machine under the asymmetric air gap," *IEEE Trans. Ind. Electron.*, vol. 65, no. 12, pp. 9843–9852, Dec. 2018.

[110] W. Sun, Q. Li, L. Sun, L. Zhu, and L. Li, "Electromagnetic analysis on novel rotor-segmented axial-field SRM based on dynamic magnetic equivalent circuit," *IEEE Trans. Magn.*, vol. 55, no. 6, Jun. 2019, Art. no. 8103105.

[111] M. L. Bash, J. M. Williams, and S. D. Pekarek, "Incorporating motion in mesh-based magnetic equivalent circuits," *IEEE Trans. Energy Convers.*, vol. 25, no. 2, pp. 329–338, Jun. 2010.

[112] W. Peng and J. Gyselinck, "Magnetic-equivalent-circuit modelling of switched reluctance machines with mutual coupling effects," in *Proc. IEEE Int. Conf. Elect. Mach.*, Lausanne, Switzerland, Sep. 2016, pp. 426–432.

[113] Q. Yu, X. Wang, and Y. Cheng, "Magnetic modeling of saliency effect for saturated electrical machines with a new calculation method," *IEEE Trans. Magn.*, vol. 52, no. 6, Jun. 2016, Art. no. 8001106.

[114] S.-H. Mao, D. Dorrell, and M.-C. Tsai, "Fast analytical determination of aligned and unaligned flux linkage in switched reluctance motors based on a magnetic circuit model," *IEEE Trans. Magn.*, vol. 45, no. 7, pp. 2935–2942, Jul. 2009.

[115] N. Radimov, N. Ben-Hail, and R. Rabinovici, "Simple model of switched-reluctance machine based only on aligned and unaligned position data," *IEEE Trans. Magn.*, vol. 40, no. 3, pp. 1562–1572, May 2004.

[116] D. S. Mihic, M. V. Terzic, and S. N. Vukosavic, "A new nonlinear analytical model of the SRM with included multiphase coupling," *IEEE Trans. Energy Convers.*, vol. 32, no. 4, pp. 1322–1334, May 2017.

[117] J. Du, D. Liang, and X. Liu, "Performance analysis of a mutually coupled linear switched reluctance machine for direct-drive wave energy conversions," *IEEE Trans. Magn.*, vol. 53, no. 9, Dec. 2017, Art. no. 8108110.

[118] G. Liu, S. Jiang, W. Zhao, and Q. Chen, "Modular reluctance network simulation of a linear permanent-magnet vernier machine using new mesh generation methods," *IEEE Trans. Ind. Electron.*, vol. 64, no. 7, pp. 5323–5332, Jul. 2017.

[119] J. Perho *et al.*, "Reluctance network for analysing induction machines," Ph.D. dissertation, Dept. Elect. Commun. Eng., Helsinki Univ. Technol., Espoo, Finland, 2002.

[120] P. Sewell, K. Bradley, J. Clare, P. Wheeler, A. Ferrah, and R. Magill, "Efficient dynamic models for induction machines," *Int. J. Numer. Modelling: Electron. Netw., Devices Fields*, vol. 12, no. 6, pp. 449–464, Nov. 1999.

[121] A. D. Callegaro, J. Liang, J. W. Jiang, B. Bilgin, and A. Emadi, "Radial force density analysis of switched reluctance machines: The source of acoustic noise," *IEEE Trans. Transp. Electrific.*, vol. 5, no. 1, pp. 93–106, Dec. 2018.

[122] J. Dong *et al.*, "Hybrid acoustic noise analysis approach of conventional and mutually coupled switched reluctance motors," *IEEE Trans. Energy Convers.*, vol. 32, no. 3, pp. 1042–1051, Feb. 2017.
[123] M. Amrhein, "Induction machine performance improvements: Design-oriented approaches," Ph.D. dissertation, Dept. Elect. Comput. Eng., Univ. Illinois at Urbana-Champaign, Champaign, IL, USA, 2007.
[124] K. Nakamura, S. Fujio, and O. Ichinokura, "A method for calculating iron loss of an SR motor based on reluctance network analysis and comparison of symmetric and asymmetric excitation," *IEEE Trans. Magn.*, vol. 42, no. 10, pp. 3440–3442, Oct. 2006.

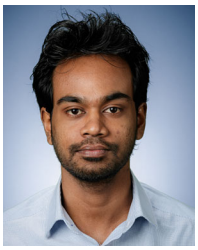

GAYAN WATTHEWADUGE (Member, IEEE) received the B.Sc and M.Sc degrees from the University of Moratuwa, Sri Lanka and the University of Manitoba, Winnipeg, MB, Canada in 2016 and 2019, respectively. He is currently a Ph.D. student in Department of Electrical and Computer Engineering at McMaster University, Hamilton, ON, Canada. His research interests includes design, analysis and modeling of electrical machines, power electronics for motor drive applications and, power distribution system architectures for electric and more electric aircraft.

Mr. Watthewaduge is serving as an Active Reviewer in IEEE publications including IEEE TRANSACTIONS OF TRANSPORTATION ELECTRIFICATION and IEEE TRANSACTIONS ON ENERGY CONVERSION.

EHAB SAYED (Member, IEEE) received the B.Sc. degree in electrical engineering with the highest distinction from Shoubra Faculty of Engineering, Benha University, Egypt, in 2010. He worked as a teaching and research assistant at the same faculty until 2016. In 2016, he received the M.Sc. degree in electrical engineering, electrical machines and drive systems specialization. He joined McMaster University in 2016 to pursue a Ph.D. degree in electrical engineering. He has been involved in many industrial projects where he designed various types of electric machines. He received a Ph.D. degree in electrical engineering in 2019. He is currently a Postdoctoral Fellow at McMaster Automotive/Aerospace Resource Centre where his research interest is the design of electric machines for automotive/aerospace applications.

ALI EMADI (Fellow, IEEE) received the B.S. and M.S. degrees in electrical engineering with highest distinction from Sharif University of Technology, Tehran, Iran, in 1995 and 1997, respectively, and the Ph.D. degree in electrical engineering from Texas A&M University, College Station, TX, USA, in 2000. He is the Canada Excellence Research Chair Laureate at McMaster University in Hamilton, Ontario, Canada. He is also the holder of the NSERC/FCA Industrial Research Chair in Electrified Powertrains and Tier I Canada Research Chair in Transportation Electrification and Smart Mobility. Before joining McMaster University, Dr. Emadi was the Harris Perlstein Endowed Chair Professor of Engineering and Director of the Electric Power and Power Electronics Center and Grainger Laboratories at Illinois Institute of Technology in Chicago, where he established research and teaching facilities as well as courses in power electronics, motor drives, and vehicular power systems. He was the Founder, Chairman, and President of Hybrid Electric Vehicle Technologies, Inc. (HEVT) — a university spin-off company of Illinois Tech. Currently, he is the President and Chief Executive Officer of Enedym Inc. and Menlolab Inc.—two McMaster University spin-off companies. He is the principal author/coauthor of over 500 journal and conference papers as well as several books including *Vehicular Electric Power Systems (2003)*, *Energy Efficient Electric Motors (2004)*, *Uninterruptible Power Supplies and Active Filters (2004)*, *Modern Electric, Hybrid Electric, and Fuel Cell Vehicles (2nd ed, 2009)*, and *Integrated Power Electronic Converters and Digital Control (2009)*. He is also the Editor of the *Handbook of Automotive Power Electronics and Motor Drives (2005)* and *Advanced Electric Drive Vehicles (2014)*. He is the Co-Editor of the *Switched Reluctance Motor Drives (2018)*. Dr. Emadi was the Inaugural General Chair of the 2012 IEEE Transportation Electrification Conference and Expo (ITEC) and has chaired several IEEE and SAE conferences in the areas of vehicle power and propulsion. He was the founding Editor-in-Chief of the IEEE TRANSACTIONS ON TRANSPORTATION ELECTRIFICATION from 2014 to 2020.

BERKER BILGIN (Senior Member, IEEE) received the Ph.D. degree in electrical engineering from Illinois Institute of Technology, Chicago, IL, USA, in 2011, and the MBA degree from DeGroote School of Business, McMaster University, Hamilton, ON, Canada, in 2018.

Dr. Bilgin is an Assistant Professor with the Department of Electrical and Computer Engineering (ECE), McMaster University. He is the Co-Founder and the Vice President of Engineering of Enedym Inc., Hamilton, ON, Canada, which is a spin-off company of McMaster University. Enedym specializes in electric machines, electric motor drives (EMDs), advanced controls and software, and virtual engineering. Dr. Bilgin has authored and co-authored 94 journals and conference papers and 3 book chapters. He is the Principal Inventor/Co-Inventor of ten patents and pending patent applications. His current research interests include electric machines, switched reluctance motor (SRM) drives, acoustic noise and vibration analysis and reduction, and power electronics and EMDs. He is the Lead Editor and author of the textbook titled *SRM Drives: Fundamentals to Applications*.

Dr. Bilgin was the Elected General Chair of the 2016 IEEE Transportation Electrification Conference and Expo (ITEC). He also serves as an Associate Editor for the IEEE TRANSACTIONS ON TRANSPORTATION ELECTRIFICATION.